AIP | Review of Scientific Instruments

Design and performance of a sub-nanoradian resolution autocollimating optical lever

R. Cowsik, R. Srinivasan, S. Kasturirengan, A. Senthil Kumar, and K. Wagoner

Citation: Review of Scientific Instruments **78**, 035105 (2007); doi: 10.1063/1.2714044
View online: http://dx.doi.org/10.1063/1.2714044
View Table of Contents: http://scitation.aip.org/content/aip/journal/rsi/78/3?ver=pdfcov
Published by the AIP Publishing

Design and performance of a sub-nanoradian resolution autocollimating optical lever

R. Cowsik,[a] R. Srinivasan, S. Kasturirengan, A. Senthil Kumar, and K. Wagoner
McDonnell Center for the Space Sciences, and The Department of Physics, Washington University, St. Louis, Missouri 63130

(Received 30 November 2006; accepted 5 February 2007; published online 15 March 2007)

Precision goniometry using optics has the advantage that it does not impose much stress on the object of investigation and, as such, is adopted extensively in gravitational wave detection, in torsion balances investigating fundamental forces, in specialized studies of biological samples, and it has potential applications in condensed matter physics. In this article we present the considerations that go into designing optical levers and discuss the performance of the instrument we have constructed. We motivate the design by considering an idealized setup and the limitations to the angular resolution induced by statistical fluctuations of the photon count rate and diffraction at the apertures. The effects of digitization of the count rate and of the spatial location of the photons on the image plane motivating the actual design are discussed next. Based on these considerations, we have developed an autocollimating optical lever which has a very high resolution and dynamic range. An array of 110 slits, of 90 μm width and a pitch of 182 μm, is located in the focal plane of a field lens, of focal length 1000 mm, and is illuminated by a CCFL tube. This array is imaged back onto the focal plane after retroreflection from a mirror placed just beyond the lens. The image is recorded on a linear charge-coupled device array at the rate of 1000 images/s and is processed through a special algorithm to obtain the centroid. The instrument has a centroid stability of $\sim 3 \times 10^{-10}$ rad Hz$^{-1/2}$ and a dynamic range of $\sim 10^7$. © *2007 American Institute of Physics.*
[DOI: 10.1063/1.2714044]

I. INTRODUCTION

Optical levers have been used as angle measuring devices for a long time, with recorded history dating back to the 18th century in the works of Coulomb and Cavendish. They have a high angular resolution and apply negligible torques on the object whose angular orientation is being measured. The early applications in the field of electromagnetism and gravitation were taken up again by Eötvos, who used an optical lever in an autocollimating configuration to study, with a torsion balance, gradients in terrestrial gravity and set bounds on the violation of Einstein's principle of equivalence of inertial and gravitational masses.

With the advent of photosensitive electronic detectors the angular resolution improved dramatically, especially by the efforts of Jones and Richards[1] and by Roll, Krotkov, and Dicke.[2] After these early developments, Cowsik, Krishnan, and others[3] implemented the Dicke design, which involves chopping of a diffraction limited image of a slit by a vibrating wire to achieve a resolution of $\sim 10^{-9}$ rad Hz$^{-1/2}$ and a dynamic range of ~ 1000. In 1992 Cowsik conceived of an optical lever in which the diffraction limited images of the slits were profiled using a charge-coupled device (CCD) and a preliminary version of the design was implemented, achieving a resolution of $\sim 10^{-8}$ rad Hz$^{-1/2}$.[4] More recently, during the last decade, considerable interest in optical goniometers has been evoked with a variety of applications in mind:[5–27] Studies of gravitation, Casimir forces and searches for new forces not discovered as yet, stabilizing the optics of the LIGO-interferometer for the detection of gravitational waves, materials science and condensed matter physics, and nanomechanics are some of the areas in which optical levers play an important role today.

This article is devoted to the description of a CCD-based autocollimating optical lever that has a resolution of $\sim 10^{-10}$ rad Hz$^{-1/2}$ and a dynamic range exceeding a few million. Even though we have developed this instrument with applications to fundamental physics[11] and geophysics[12,28] in mind, it is versatile and can be deployed for other applications as well. In Sec. II we discuss broadly the design considerations that went into the construction of this optical lever; indeed, some of these considerations are important for the functioning of any optical lever. In Sec. III we describe the optical lever that has been fabricated by our group. Finally, in Sec. IV we describe the performance of the instrument and comment on possible avenues for improvement.

II. DESIGN CONSIDERATIONS

A. Basics

The general layout of an optical lever in the autocollimating configuration is shown in Fig. 1. A source of light, F, illuminates a slit S, located effectively at the focal plane of a field lens L. In order to keep the source and the image as close to the optic axis as possible, it may be necessary to use a flat mirror M_1 to reflect the light from the source, so that

[a]Electronic mail: cowsik@physics.wustl.edu

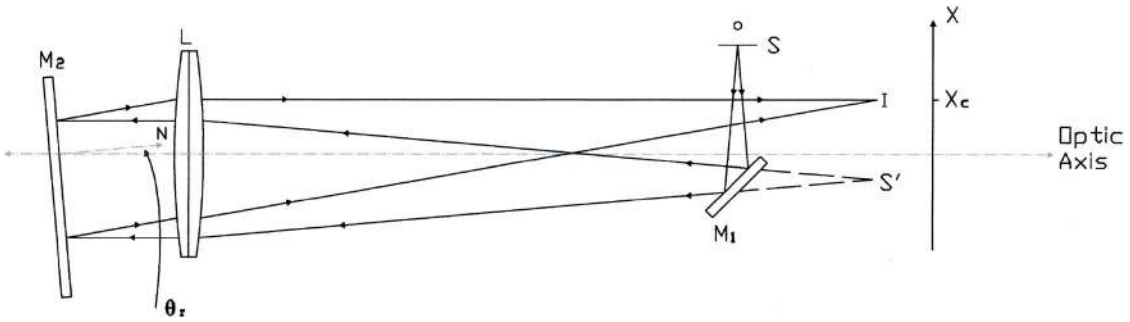

FIG. 1. Schematic diagram of the autocollimating optical lever.

the virtual image S' is located in the focal plane. The collimated beam emerging from the field lens gets reflected off a flat mirror, M_2, fixed to the object whose angular position is to be determined. The normal to this mirror N, makes an angle θ_r with respect to the optic axis of the lens. The light beam after reflection returns through the field lens and forms a well-focused image I of unit magnification on a position sensitive detector. The aim of the optical lever is to measure the angle between the optic axis of the lens and the normal to the mirror.

The autocollimating configuration for the optical lever ensures the stability of the image against small deviations in the length of the optical path. Furthermore, the measured angle is insensitive to thermal expansion of the device. These aspects have been well recognized and the autocollimating configuration is generally adopted in modern optical devices.

Once a good image of the well-illuminated light slit is obtained, the angle between the normal to the mirror and the optic axis is simply related to the distance to the centroid of the image from a fiducial point. The diffraction broadened image is shown schematically in Fig. 2. Referring to this figure, the angle θ_r is given by

$$\theta_r = x_c/2f. \tag{1}$$

Here, x_c is the location of the centroid of the image and f is the focal length of the field lens.

In order to discuss the various factors which affect the resolution of the lever, let us investigate the idealized situation where we know the exact location of impact of all the photons on the focal plane. We will also assume, conveniently, that the image has a Gaussian profile,

$$n(x)dx = \frac{N_0 dx}{\sqrt{2\pi\sigma^2}} e^{-(x-x_0)^2/2\sigma^2}. \tag{2}$$

Here, N_0 is the total number of photons in the image collected per second, $n(x)$ is the number density per unit x at x, σ is the rms width of the image, and x_0 is the median. (The non-Gaussian diffraction tails of the distribution are truncated along with the general background as described later.) Let us define the various moments of this distribution,

$$m_i = \int x^i n(x)dx. \tag{3}$$

The location of the centroid is given by

$$x_c = \frac{m_1}{m_0} \equiv \frac{\int_{-\infty}^{\infty} \frac{xN_0}{(2\pi\sigma^2)^{1/2}} e^{-x(x-x_0)^2/2\sigma^2} dx}{\int_{-\infty}^{\infty} \frac{N_0}{(2\pi\sigma^2)^{1/2}} e^{-(x-x_0)^2/2\sigma^2} dx} = \frac{N_0 x_0}{N_0} = x_0, \tag{4}$$

as expected. Now, what is the uncertainty in the observational estimate of x_c? Consider a narrow strip of width Δx at x (see Fig. 2). The mean number of photons in the strip will be $n(x)\Delta x$. The actual number will exhibit Poissonian fluctuations about this mean. For $n(x)\Delta x \gg 1$ the uncertainty in the number is $\sim[n(x)\Delta x]^{1/2}$, and this will contribute an uncertainty $\sim x[n(x)\Delta x]^{1/2}$ to the moment m_1. These uncertainties at different parts of the image will not be correlated; accordingly, they will add in quadrature. Thus, in an idealized detector in which the position x of each photon generating a count is known exactly, we have

$$\Delta m_1^2 = \pm \sum_{\lim \Delta x \to 0} [x\{n(x)\Delta x\}^{1/2}]^2$$

$$= \pm \int_{-\infty}^{\infty} x^2 n(x)dx = \pm m_2 = \pm N_0(\sigma^2 + x_0^2). \tag{5}$$

Thus,

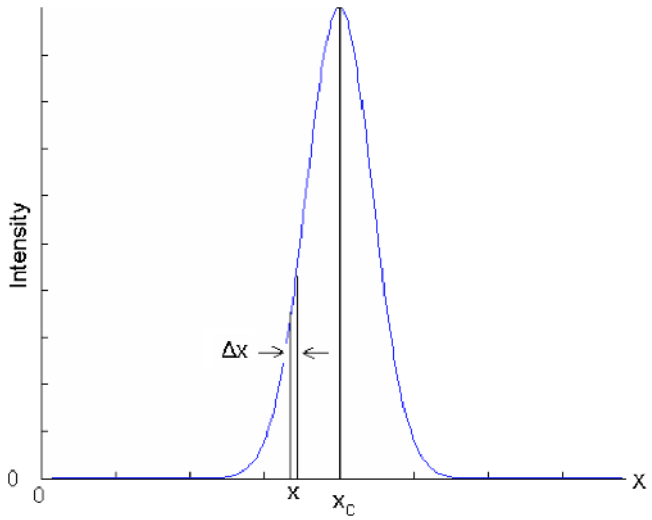

FIG. 2. Diffraction limited image of a single slit.

$$x_c \pm \Delta x_c = \frac{m_1 \pm [m_2]^{1/2}}{m_0} = x_0 \pm \frac{(\sigma^2 + x_0^2)^{1/2}}{N_0^{1/2}}. \quad (6)$$

This equation indicates that the uncertainty Δx in the measurement of x_c decreases as N_0 increases and as σ and x_0 decrease. Let us consider these parameters one at a time. The total number of photons N_0 depends on the width and length of the slit, w and l, the intensity of its illumination, which will determine its effective temperature, and the duration of the observation, Δt,

$$N_0 = lwI(T)\Delta\Omega. \quad (7)$$

Note that I is the intensity of illumination in photons per unit area, per unit solid angle, per unit time, and T is the effective temperature of the source which is below 2000 K for thermal sources, and imposes a restriction on how high N_0 can be. I therefore is essentially given by the blackbody law for photon intensities above the threshold frequency for detection but with a large dilution factor related to the transfer of light from the source onto the slit, along the optical path and back to the position sensitive detector, say a CCD camera. Even though in principle this limitation might be overcome by using coherent light from a laser, it will cause problems because the main beam with intensity I would interfere with scattered beam from the various surfaces, say of strength I_s, to produce a high background of intensity $\sim(I \cdot I_s)^{1/2}$. The value of $\Delta\Omega$ is set essentially by the largest F-number in the system, where $F=f/D$, where D is the diameter of the mirror M_2 or the lens L, whichever is smaller, and f is the focal length of the field lens; $\Delta\Omega \approx 1/F^2 \approx D^2/f^2$.

Returning to our consideration of Eq. (6), the width of the image σ is the sum of the width of the slit and the width of the diffraction pattern

$$\sigma \approx w + 2\left(\frac{1.22\lambda}{D} f\right) \approx w + 2.4\lambda f/D. \quad (8)$$

Because we do not know the location of the centroid *ab initio*, the choice for the fiducial location from which all x measurements are carried out cannot be brought closer than σ. In other words, the best possible choice is

$$x_0 \approx \sigma. \quad (9)$$

Thus, the expected resolution is of the order of

$$\Delta x_c \approx \left\{\frac{\sigma^2 + x_0^2}{N_0}\right\}^{1/2} \approx \left\{\frac{2\sigma^2}{N_0}\right\}^{1/2}. \quad (10)$$

Thus, any attempt to increase N_0 by increasing w in order to improve the resolution will be frustrated by a more rapid increase of $\sigma^2 \sim \omega^2$ in the numerator. Nor can we reduce the width of the slit indefinitely. To appreciate this, we note that the diffraction at the slit will spread the beam over an angle θ_s which has to be kept smaller than the F-number of the field lens, lest one lose the outer regions of the beam and thus reduce N_0. Accordingly,

$$\theta_s \sim \frac{2\lambda}{w} < \frac{D}{f} \text{ or } w > \frac{2\lambda f}{D}, \quad (11)$$

$$\Delta\theta \approx \frac{\Delta x_c}{2f} \geq \frac{1}{2f}\left[\frac{2(2\lambda f/D + 2.4\lambda f/D)^2}{N_0}\right]^{1/2}$$
$$\approx (3\lambda/D)/N_0^{1/2} \text{ rad Hz}^{-1/2}. \quad (12)$$

The import of this result is intuitively clear: the scale for the angular resolution is set by the diffraction at the mirror with aperture D and the angular resolution improves as the square root of the number of photons detected. Furthermore, when we set l also equal to $\omega \approx 2\lambda f/D$, as appropriate to a linear CCD array acting as the detector, and set $\Delta\Omega \approx D^2/f^2$ in the expression for N_0 in Eq. (7), we find Eq. (12) now becomes

$$\Delta\theta \geq 1.5/(ID^2)^{1/2}. \quad (13)$$

Recalling that I is the intensity of illumination dependent on the temperature of the source and the efficiency of photon transport and detection, Eq. (13) indicates that there exists a practical limit to the resolution of autocollimating optical levers. In fact, because Eq. (13) was derived for an idealized detector with 100% efficiency and perfect spatial resolution, this equation represents a strict upper bound on the resolution of the autocollimator. For typical table-top systems in a laboratory, for example using a linear CCD array as the detector, the resolution $\Delta\theta$ is rarely better than $\sim 10^{-9}$ rad Hz$^{-1/2}$. The dynamical range of these systems, R, is also limited typically to $\sim\omega/2f \sim \lambda/D$, the diffraction angle at the aperture, beyond which the resolution decreases as a consequence of the increase of x_0 in Eq. (10). In the analysis presented above, we have assumed an idealized detector and that the position of every photon is accurately known and the intensity is measured precisely. The effects of spatial and intensity digitization will be briefly discussed later in Sec. II D.

B. Toward the design of a higher resolution autocollimator

Consider a sequence of k slits, each identical to the one discussed in Sec. II A, with the array having a pitch a. The location of the centroid of the array x_c is now given by

$$x_c = \frac{\sum m_{1i}}{\sum m_{0i}} = \frac{\sum x_{0i} N_{0i}}{\sum N_{0i}}. \quad (14)$$

Here, m_{0i} and m_{1i} are the zeroth and first moments of the ith image, and $x_{0i}=x_0+(i-1)a$ is the median of the ith image. Now, assuming for simplicity that $N_{0i} \approx N_0$ for all i, we get

$$x_c = \left\{kx_0N_0 + N_0a\sum_{k=2}^{k}(i-1)\right\}/kN_0 = x_0 + (k-1)a/2, \quad (15)$$

as expected. However, note that

$$\langle \Delta x_c \rangle^{1/2} = \left\{\sum_{i=1}^{k} N_{0i}[\sigma^2 + \{x_0 + (i-1)a\}^2]\right\}^{1/2} \Big/ \sum_{i=1}^{k} N_{0i}$$
$$\approx \left\{k(\sigma^2 + x_0^2) + k(k-1)x_0a + \frac{k(k-1)(2k-1)}{6}a^2\right\}^{1/2} \Big/ kN_0^{1/2}. \quad (16)$$

TABLE I. Properties of CCD camera: Perkin Elmer LD3523PGK-011.

Pixel size	14 μm square
Number of pixels	2048
Output rate	20 MHz
dc supply	12–24 V
Interface	CameraLink, IMAQ PCI-1428
Trigger external	~1000 frames/s
Digitization of intensities	8 bits
Well depth	~64 000 electrons ~ 2^{16}
Operating level	~32 000 electrons ~ 2^{15}
	$N_{\text{bits}} \sim 1.6 \log 32\,000 \sim 7-8$ bit
No. of electrons/bit	≈100

The third term inside the brackets indicates that

$$\langle \Delta x_c^2 \rangle^{1/2} \sim \frac{k^{1/2} a}{N_0^{1/2}}, \tag{17}$$

for large k. Thus, by merely having multiple slits we are actually degrading the measurement accuracy.

C. Toward a solution

Now, let us consider the image of the same array of slits and a set of fiducial locations y_i also with the same pitch, that is

$$y_i - y_{i-1} \approx a. \tag{18}$$

The centroids and their corresponding uncertainties, of the images, each measured from their corresponding fiducials at y_i, are given by

$$x_{ci} \pm \Delta x_{ci} = x_{0i} \pm \frac{(\sigma^2 + x_{0i}^2)^2}{N_{0i}^{1/2}}, \tag{19}$$

with obvious notation, in parallel to that in Sec. II B except that the ith image has its own fiducial located at y_i. Averaging over the k peaks, we get

$$\bar{x}_{ci} \pm \langle \Delta x_{ci}^2 \rangle^{1/2} \approx \frac{\sum x_{0i}}{k} \pm \frac{\{\sum_{i=1}^{k} (\sigma^2 + x_{0i}^2)^{1/2}\}^{1/2}}{k N_0^{1/2}}$$

$$\approx \frac{\sum x_{0i}}{k} \pm \frac{(\sigma^2 + x_0^2)^{1/2}}{k^{1/2} N_0^{1/2}}. \tag{20}$$

Adding to this the mean location of the fiducials,

$$x_c \pm \Delta x_c = \frac{\sum y_i + x_{0i}}{k} \pm \frac{(\sigma^2 + x_0^2)^{1/2}}{k^{1/2} N_0^{1/2}} = x_c \pm \frac{(\sigma^2 + x_0^2)^{1/2}}{k^{1/2} N_0^{1/2}}. \tag{21}$$

We have thus recovered the original location of the centroid and gained in resolution by a factor of $k^{-1/2}$. The summing of the locations of the fiducials does not add to the uncertainty of the centroid. The range of x_c values over which accurate measurements can be carried out is given by the difference between the length of the photon detector and the width of the array of slits,

$$s = y_m - y_0 - (k-1)a. \tag{22}$$

This corresponds to an angular range of

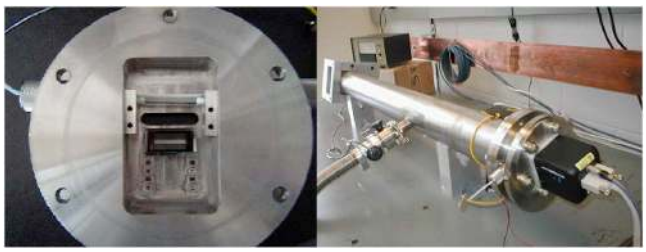

FIG. 3. On the left is the plate, housing the compact fluorescent lamp, the array of slits forming a grating and the 45° mirror. Notice the reflection in the mirror. The grating, which is too fine to be seen, is directly in front of the bulb. The window between the grating and the mirror allows the image to reach the CCD. On the right is the assembled autocollimator. The bellows that connects the autocollimator to the vacuum pump is seen coming from the left. In the foreground is the CCD camera that is connected to a PC for analysis.

$$\theta_{\text{range}} = s/2f = [y_n - y_0 - (k-1)a]/2f. \tag{23}$$

Thus, the dynamical range is extended considerably.

D. Some further considerations

In general, besides the images of the slits whose intensities are given by $n_i(x)$ [see Eq. (2)], there will be a background of approximately constant intensity b. Indeed, the background could also have important contributions from the Lorentzian tails of the images. This background, b, and its fluctuations $\pm\Delta b$ will shift the centroid and also add to its uncertainty. When we have sharp and intense images, it would be worthwhile to subtract this background. If c_i is the number of photon counts in a narrow bin with corresponding background b and Δb, we may carry out the centroiding process described earlier using the background subtracted c_i^* defined by

$$\begin{aligned} c_i^* &= c_i - (b + 3\Delta b) \quad \text{for } c_i^* > 0 \\ &= 0 \qquad\qquad\quad \text{for } c_i^* < 0 \end{aligned}. \tag{24}$$

When working with CCD arrays, we need to choose the image width approximately in relation to the width of the individual pixels. The effects of spatial digitization of the image may be kept small by using the following prescription. The shape of the image around the peak may be characterized by its various moments, m_ν, like total number, centroid, width, skewness, kurtosis, etc. The number of spatially pixelized intensities of each image should be chosen to be larger than the number of parameters needed to characterize the image,

$$n_{\text{pix}} > n_{\text{parameter}} \approx 4. \tag{25}$$

Thus, a choice of $n_{\text{pix}} \approx 6$ or 7 should be sufficient to generate negligible errors of spatial digitization.

The output of the individual pixels will pass through an analog-to-digital converter (ADC) and will be read off in a digitized form. In order to estimate the resolution required for the ADC, recall that when on average c photons are counted, there would be an uncertainty $c^{1/2}$ in the intensity or a fractional error $\Delta_s \approx c^{1/2}/c = c^{-1/2}$. If 1 bit in the ADC corresponds to n_d photon counts, the digitization will yield $(c \pm c^{1/2})/n_d$ digital counts c_d. The uncertainty in the digitiza-

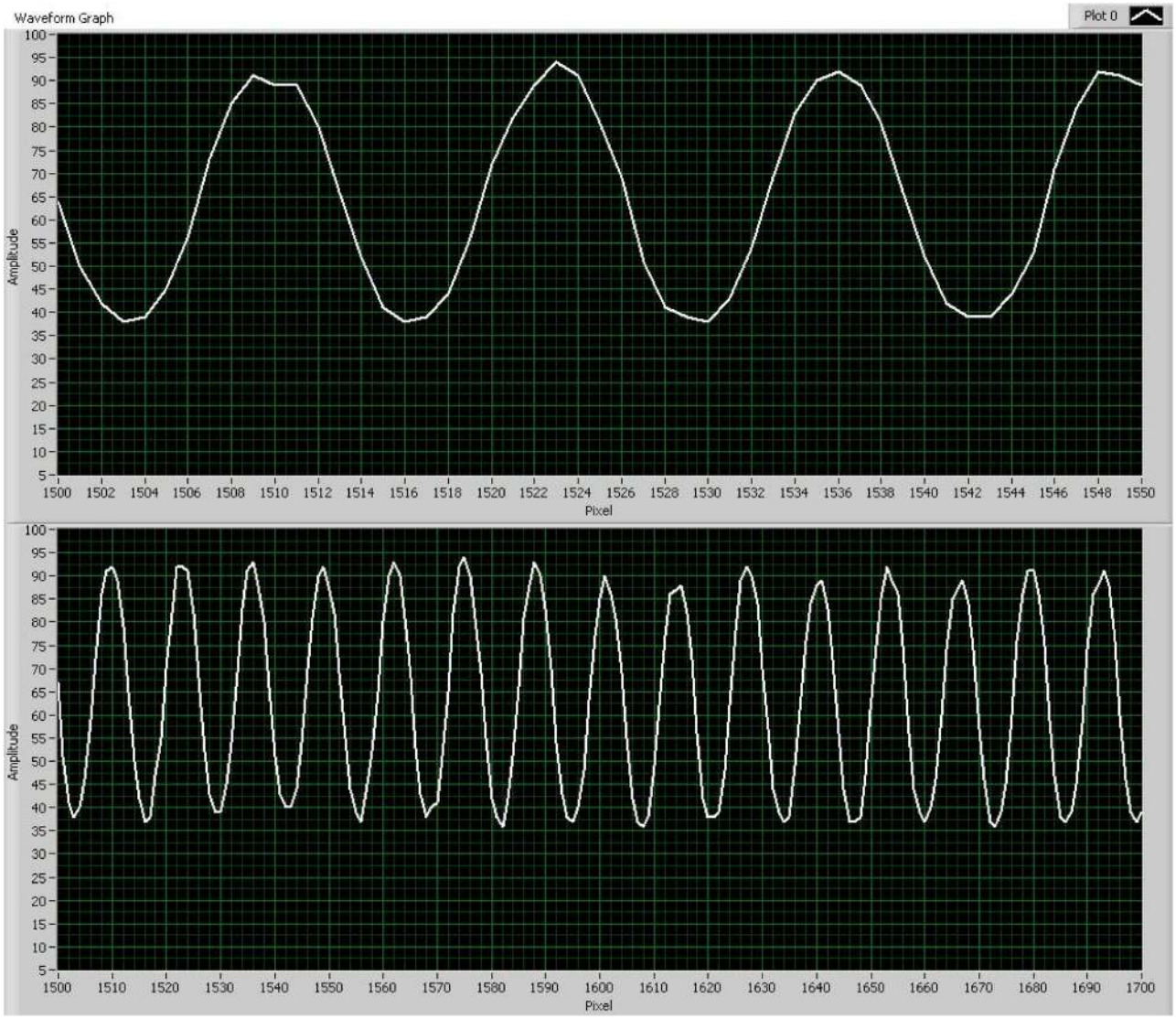

FIG. 4. Intensity of the image vs pixel number for linescan CCD is shown in an expanded scale on the top panel over a range of 50 pixels and over a range of 200 pixels in the lower panel.

tion process is 1 digitized count in N_{bit}, the binary order of the ADC, which is equivalent to n_d in the photon counts. Thus, the fractional digitization error is

$$\Delta_d = \frac{1}{2^{N_{bit}}}. \tag{26}$$

In order that the digitization error does not add significantly to the error budget we have to choose $\Delta_d < \Delta_c$,

$$\frac{1}{N_{bit}} < c^{-1/2} \quad \text{or} \quad N_{bit} > 1/2(\log c/\log 2)$$
$$\approx 1.6 \log_{10} c \sim 8, \quad \text{for } c \sim 10^5. \tag{27}$$

The next point to consider is the right choice for the aspect ratio (l/w) of the slit/image. In the context of the CCD camera acquiring the image, this issue is closely linked with the reading and processing time of the image. Suppose the array of images is along the "row" direction and the height "l" is along the "column" direction of the CCD. The length of the row, i.e., the number of columns, is given by $n_c = ka/p$, where p is the pixel width, k is the number of images in the array, and a is the pitch, so that ka is the length of the image array. Considering the standard row-transfer and serial readout protocol of the CCD camera, the time required for reading a row and processing it may be written as

$$\tau \approx \frac{ka}{p}\Delta\tau, \tag{28}$$

where $\Delta\tau \sim 1-2$ μs is the typical time needed for the serial readout and process of a pixel from the register. If the image is of height l, then there are $n_r = l/p$ rows in it and the total time needed to process the image is

$$\tau_{tot} \approx n_r\tau = n_r n_c \Delta\tau. \tag{29}$$

Here, we have neglected the very short time needed for shifting the row of charges toward the register. Now, this time interval τ_{tot} is the time for which the electrons in the CCD well are allowed to accumulate, the "integration time," as it is often called. The number of electrons accumulated may be estimated, using Eq. (7), as

$$n_e = I(T)\Delta\Omega p^2\ \tau_{\rm tot}. \tag{30}$$

For an efficient and effective operation

$$n_e \leq 0.7 n_w, \tag{31}$$

where n_w is the well depth of the CCD. Thus, Eqs. (28)–(30) imply

$$n_r \leq n_w/[I\Delta\Omega p^2 n_c \Delta\tau] \tag{32}$$

or

$$l < n_\omega p/[I\Delta\Omega p^2 n_c \Delta\tau]. \tag{33}$$

III. IMPLEMENTATION OF THE DESIGN CONCEPTS

The image acquisition system is a digital linescan camera, Perkin Elmer mdel-LD3523. It has one row, or $n_r=1$, of 2048 pixels each of size 14×14 μm, thus covering a length of ~28 mm; its characteristics are listed in Table I. An array of 110 slits, each of width 90 μm, is separated by a dark region of width 92 μm, so that the pitch is 182 μm. Thus, the image of each slit is sampled by 13 pixels. The illumination is provided by a CCFL-JKL-lamp 560-BXA-12529, and a mirror held at 45° with respect to the optic axis reflects the light from the slits toward an achromat 1000 mm away so that the virtual image of the slits is in the focal plane of the lens. Photographs of the various parts of the autocollimating optical lever are shown in Fig. 3. The image acquisition and the centroiding routines are implemented through LabView.

A typical example of the image is displayed in Fig. 4, with two levels of magnification: 200 and 50 pixels. The software used for the centroiding along the lines outlined in the design was implemented in a straightforward manner. For the initial testing the optical lever was made to view a flat mirror fixed to it. The optical path was evacuated to ~1 Torr to reduce the effects of turbulence; the lever was thermally insulated with ~50 mm of Styrofoam and suspended by bungee cords to minimize vibrations.

IV. COMMENTS ON THE PERFORMANCE AND FUTURE DEVELOPMENTS

The performance characteristics are best displayed as the Fourier transform of the signal; this is done in Figs. 5 and 6. Note that in Fig. 5 the angular resolution at high frequencies up to ~20 Hz is $\sim 2\times 10^{-10}$ rad Hz$^{-1/2}$ but degrades below $\sim 10^{-2}$ Hz. The low-frequency region is displayed on a log-log graph in Fig. 6. From the best fit to this curve (not shown) we note that the resolution can be parametrized as

$$\Delta\theta = 2\times 10^{-10}(0.01\ \text{Hz}/\nu)\text{rad Hz}^{-1/2},\quad \text{for } \nu < 10^{-2}\ \text{Hz}. \tag{34}$$

The resolution degrades with decreasing frequency, probably because of drifts and fluctuations in the temperature, pressure, and other parameters of the environment. Nevertheless, for observations of periodic motions even at low frequencies, the optical lever provides adequate resolution. The typical bandwidth of observation at a frequency ν is $\sim\nu/Q$, where Q is the quality factor of the oscillator under study. The effective amplitude of oscillation that can be detected is given by

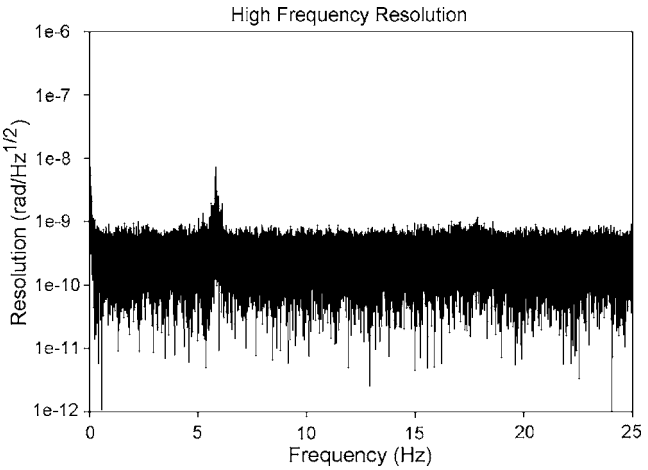

FIG. 5. A power spectrum of the background noise in the angular orientation of a fixed mirror observed with the autocollimating optical lever is shown. The spike comes at the natural frequency of the bungee cords from which the autocollimator was suspended. Also present is some enhanced power at very low frequencies; this is due to changing environmental conditions in the laboratory where these data were recorded.

$$\Delta a \approx \Delta\theta\left(\frac{\nu}{Q}\right)^{1/2} \approx 2\times 10^{-12}\frac{\text{rad}}{(Q\nu)^{1/2}}. \tag{35}$$

Thus, at $\nu\sim 10^{-4}$ Hz and with $Q\sim 100$ an amplitude of 2×10^{-11} rad could be measured.

In Fig. 7 we show the phase of the calibration signal as a function of frequency. Note that the phase is completely random and extends from $+\pi$ to $-\pi$. This indicates that the noise that is present in the signal has no correlations whatsoever and is very similar to thermal noise, even though the spectrum shows enhancement at low frequencies.

We may define the dynamical range of the instrument as the ratio of the maximum angle to the minimum angle that can be measured, or, in other words, the ratio of range to the resolution. If the CCD array is of length $N_{\rm max}$ and the image length is n_c, the maximum angle deviation that can be measured is

$$\theta_{\rm max} = \pm (N_{\rm max} - n_c)p/2f. \tag{36}$$

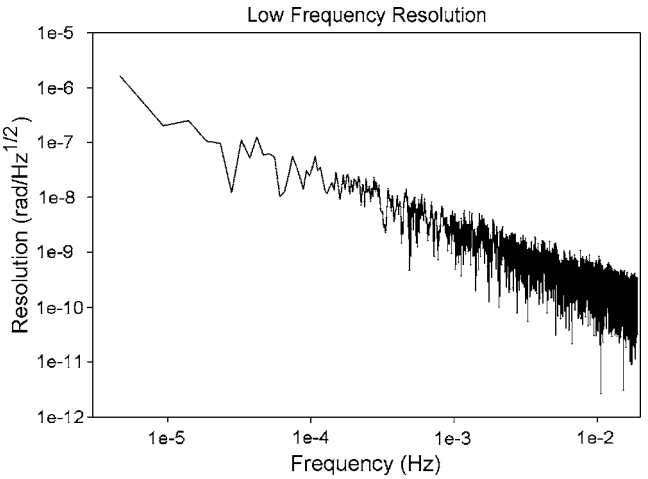

FIG. 6. Resolution of autocollimator at lower frequencies, estimated from observations of a fixed mirror.

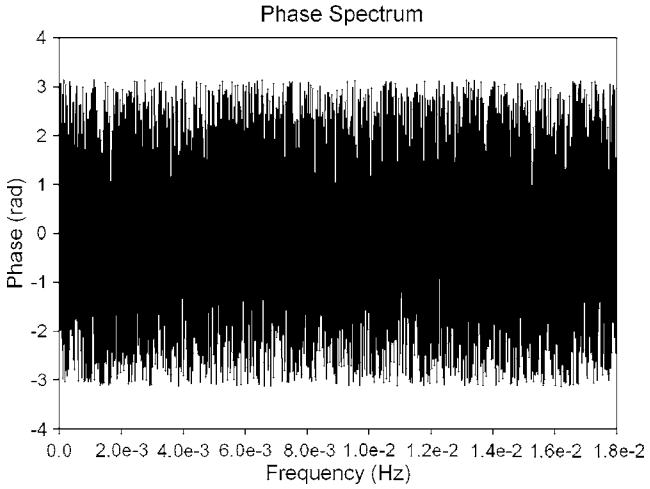

FIG. 7. Phase distribution of background signal. Notice that the signal is distributed uniformly from $-\pi$ to π with no correlations.

For the instrument we have developed $N_{\max}=2k$, $n_c=1430$, $p=13$ μm, and $f=10^6$ μm; these parameters yield $\Delta_{\max}\approx 2\times 10^{-3}$ rad. Taking the resolution $\Delta\theta$ nominally to be $\sim 2\times 10^{-10}$ rad Hz$^{-1/2}$ and the dynamic range $R\sim 10^7$, the import of Eq. (36) is essentially the same as that given in Eq. (23).

Finally, we may consider possible extensions of this optical lever for measurement of two angles θ and ϕ, i.e., as a two-dimensional detector. The design of the source will be an $n\times n$ square matrix of holes, each of size 90×90 μm, say, with a pitch of 182 μm in either direction. The criterion for near saturation of the pixels during the time needed to read and analyze a frame will be met, if the array is 4×4 and the other parameters are as described before. It is easy to show, that under these conditions, the resolution will be degraded by a factor of ~ 2.6,

$$\Delta\theta\approx\Delta\phi\approx 2\times 10^{-10}\times 2.6 \text{ rad Hz}^{-1/2}$$
$$\approx 5.2\times 10^{-10} \text{ rad Hz}^{-1/2}. \quad (37)$$

Thus, it is clear that by careful planning we may develop optical levers to measure angles with extraordinary precision using CCD arrays. Indeed, with the rapid improvement of the CCD technology that is being witnessed today, the resolutions and dynamical ranges described in this article will soon be superseded.

ACKNOWLEDGMENTS

The authors thank Dr. D. Suresh and Dr. G. Rajalakshmi for their interest in the early phase of this project, and the McDonnell Center for the Space Sciences and Washington University for the support of this effort. One of us (A.S.K.) would like to thank Vellore Institute of Technology for granting leave to work on this project.

[1] R. V. Jones and J.C.S. Richards, J. Sci. Instrum. **36**, 90 (1959).
[2] P. G. Roll, R. Krotkov, and R. H. Dicke, Ann. Phys. **26**, 442 (1964).
[3] R. Cowsik, N. Krishnan, P. Saraswat, S. N. Tandon, S. Unnikrishnan, and U. D. Vaishnav, Indian J. Pure Appl. Phys. **27**, 691 (1989).
[4] G. Rajalakshmi, Ph.D. thesis, Bangalore University (2004).
[5] R. Cowsik, in the Special Volume of the IUCAA Dedication Seminar, edited by T. Padmanakham (New Age International Ltd., New Delhi, 1997), pp. 109–119.
[6] J. T. Dawley, G. Teowee, B. J. J. Zelinski, and D. R. Uhimann, Mater. Res. Soc. Symp. Proc. **433**, 317 (1996).
[7] R. D. Newman and M. K. Bantel, Meas. Sci. Technol. **10**, 445 (1999).
[8] H. Yamaguchi and Y. Hirayama, Technol. Rev. **2**, 25 (2004).
[9] X. Yao, D. Rector, and J. George, Appl. Opt. **42**, 2972 (2003).
[10] Z. Hu, T. Seeley, S. Kossek, and T. Thundat, Rev. Sci. Instrum. **75**, 400 (2004).
[11] E.G. Adelberger, B.R. Heckel, and A.E. Nelson, Annu. Rev. Nucl. Part. Sci. **53**, 77 (2003), APS Meeting, Dallas, April 2006 (Abstract).
[12] R. Cowsik, PNAS (in press).
[13] T. Vosegaard, V. Langer, P. Daugaard, E. Hald, H. Bildsoe, and H. Jakobsen, Rev. Sci. Instrum. **67**, 2130 (1996).
[14] R. V. Jones and J. C. S. Richards, Rev. Sci. Instrum. **70**, 1771 (1999).
[15] M. V. Kovalchuk, S. I. Zheludeva, A. Ya. Kreines, Yu. N. Shilin, N. Yu. Shilina, and V. A. Shishkov, Nucl. Instrum. Methods A **405**, 440 (1998).
[16] B. Blank *et al.*, MEDSI02, http://www.aps.anl.gov/asd/me/medsi02/papers/proceedings.html (2002).
[17] M. Tanaka and K. Nakayama, Jpn. J. Appl. Phys., Part 2 **21**, L399 (1982).
[18] J. Yuan and X. Long, Rev. Sci. Instrum. **74**, 1362 (2003).
[19] P. Suortti, J. Keyriläinen, and M. Fernández, J. Appl. Crystallogr. **37**, 62 (2004).
[20] P. Gizdulich, G. Aschero, and F. Mango, Meas. Sci. Technol. **10**, 232 (1999).
[21] J. Tsai, Opt. Eng. **43**, 737 (2004).
[22] F. Ya. Khalili, Phys. Lett. A **298**, 308 (2002).
[23] H. Lin and W. Fang, Sens. Actuators, A **105**, 1 (2003).
[24] C. Savran *et al.*, J. Microelectromech. Syst. **11**, 703 (2002).
[25] N. Bhatt, http://www.ligo.caltech.edu/~cit40m/Docs/Naman_final.pdf (2003).
[26] A. N. Korolev and A. I. Gartsuev, Meas. Tech. **47**, 1178–1183 (2004).
[27] A. Kikukawa, H. Koyanagi, K. Etoh, and S. Hosaka, Jpn. J. Appl. Phys., Part 1 **39**, 1885 (2000).
[28] R. Sugahara, K. Endo, and Y. Ohsawa, Proceedings of International Workshop on B Factories, p. 211, http://www.slac.stanford.edu/econf/C930928 (1993).